

New topological excitations and melting transitions in quantum Hall systems

Tzu-ging Lin,¹ George Simion,¹ John D. Watson,^{1,2} Michael J. Manfra,^{1,2,3,4}
Gabor A. Csathy,¹ Yuli Lyanda-Geller,^{1,2,*} and Leonid P. Rokhinson^{1,2,3,†}

¹*Department of Physics, Purdue University, West Lafayette, Indiana 47907 USA*

²*Birck Nanotechnology Center, Purdue University, West Lafayette, Indiana 47907 USA*

³*Department of Electrical and Computer Engineering,
Purdue University, West Lafayette, Indiana 47907 USA*

⁴*Department of Material Engineering,
Purdue University, West Lafayette, Indiana 47907 USA*

We discover a new topological excitation of two dimensional electrons in the quantum Hall regime. The strain dependence of resistivity is shown to change sign upon crossing filling-factor-specified boundaries of reentrant integer quantum Hall effect (RIQHE) states. This observation violates the known symmetry of electron bubbles thought to be responsible for the RIQHE. We demonstrate theoretically that electron bubbles become elongated in the vicinity of charge defects and form textures of finite size. Calculations confirm that texturing lowers the energy of excitations. These textures form hedgehogs (vortices) around defects having (lacking) one extra electron, resulting in striking strain-dependent resistivity that changes sign on opposite boundaries of the RIQHE. At low density these textures form an insulating Abrikosov lattice. At densities sufficient to cause the textures to overlap, their interactions are described by the XY-model and the lattice melts. This melting explains the sharp metal-insulator transition observed in finite temperature conductivity measurements.

Topology and symmetry define states of matter and their responses to external forces. How solids melt and become fluids, or how insulators become conductors is often controlled by the generation of topological excitations. In a magnetic field the energy spectrum of electrons is quantized into discrete Landau levels, causing a two-dimensional electron gas transitions through a variety of ground states as a function of magnetic field. When an integer number of single-particle energy levels are filled (filling factor $\nu = \Phi_0/\Phi$ is integer, where $\Phi_0 = h/e$ is a flux quanta, $\Phi = B/n$ is magnetic flux per electron, B is magnetic field and n is electron density), the Hall resistance becomes quantized in multiples of $R_q = h/e^2$ and longitudinal resistance vanishes, the hallmarks of the integer quantum Hall effect[1]. Electron-electron interactions dominate physics at low filling factors ($\nu < 1$) and the many-body ground state is a competition between fractional quantum Hall effects[2], and Wigner crystals[3]. In the 2nd Landau level ($2 < \nu < 4$) exotic even-denominator fractional quantum Hall states, possibly possessing non-Abelian excitations, are found [4]. On the 3rd and higher Landau levels ($\nu > 4$) a unidirectional charge density wave, the stripe phase, is formed near half-integer filling factors[5–7]. Between integer and half-integer filling factors another set of states characterized by Hall resistance quantized to the nearest integer value but occurring at non-integer filling factor is observed, the so-called reentrant integer quantum Hall effect (RIQHE) states[8, 9]. Here we report discovery of a new class of charged

* To whom correspondence on theory should be addressed. E-mail: yuli@purdue.edu

† To whom correspondence on experiment should be addressed. E-mail: leonid@purdue.edu

topological excitations, realized in two dimensional electron systems in the RIQHE, in which elongated bubbles of electrons form finite-size textures around charge defects.

In a two-electron ($2\bar{e}$) bubble crystal there are one- and three-electron ($1\bar{e}$ & $3\bar{e}$) charge defects. We propose that elongated bubbles form hedgehogs-like and vortex-like textures around $1\bar{e}$ & $3\bar{e}$ respectively. We show that formation of textures considerably reduce energy of charged defects. Remarkably, these topological defects are very sensitive to uniaxial strain and strain-dependent resistivity has different sign for vortex and hedgehog textures. This unique property enables detailed investigation of topological defects and a Berezinsky-Kosterlitz-Thouless-like (BKT) transition [10, 11] in the previously unexplored regime, where the relative density of topological defects with different symmetry can be tuned by magnetic field. In this regime melting is a function of several variables and forms a continuous phase boundary in the field-temperature ($B - T$) plane. At low densities these textures do not overlap. They are bound in an insulating crystal [3, 12]. At high defect density, driven either by finite temperature or magnetic field, the textures begin to overlap and their interactions define the energetics of the system. These interactions are described by XY-model and induce melting of the defect lattice. The melting described here differs from the standard BKT transition [10, 11] because these finite-size topological textures must have significant spatial overlap to induce vortex unbinding. This melting transition resembles asymptotic freedom of quarks requiring them to be "squeezed" in order to be freed[13]. Melting of the lattice of topological defects explains the sharp boundary between an insulating RIQHE state and a conducting state observed in a recent experiment[14].

Magnetoresistance in a high mobility 2D electron gas is shown in Fig. 1 for filling factors between $\nu = 4$ and 5. A well-defined stripe phase with large resistance anisotropy between $[110]$ and $[1\bar{1}0]$ crystallographic directions is seen near $\nu = 4.5$. RIQHE phases are formed near $\nu = 4.3$ and 4.7 and are marked as B_1 and B_2 on the plot. The width of RIQHE phases is temperature dependent, see Fig. 2, with the insulating state bounded by a sharp resistance peak which separates insulating and conducting phases in the (B - T) plane. The most striking feature shown in Fig. 1 is strain dependence of resistivity. Uniaxial strain is expected to introduce slight anisotropy of the exchange interaction and of the effective mass for electrons in GaAs. Indeed, for the stripe phase we see small enhancement of resistivity in $[1\bar{1}0]$ and reduction in $[110]$ consistent with expectations[15]. Unexpectedly, however, the resistance vs. strain dependence changes sign across the RIQHE states: the sign of the change of resistance with strain near $\nu = 4.33$ and 4.66 is consistent with the induced anisotropy of the exchange, while near $\nu = 4.23$ and 4.73 the sign of change is reversed, see Fig. 2.

The RIQHE state was originally suggested to be a crystal of uniformly charged bubbles holding integer number of electrons[16–21]. Electron hopping between bubbles is forbidden by Coulomb blockade and conductance vanishes as long as the bubble crystal is pinned by disorder. It is conceivable that the high temperature transition to a conducting state takes place due to trivial melting of the bubble crystal. However, the observed strain response of resistivity is incompatible with the symmetry of the bubble crystal, a bubble liquid or a uniform electron liquid, and thus, the observed metal-insulator transition cannot be attributed to the melting of the bubble crystal. In the presence of strain ε resistivity becomes anisotropic, $\rho_{ii} = \rho_{ii}^0 + \beta(\varepsilon_{ii} - \varepsilon_{jj})$, and the sign of the constant β is determined by the symmetry of the underlying state. This intrinsic parameter β has to change sign across the RIQHE state as a function of magnetic field to be consistent with the experimentally measured strain dependence of resistivity. This requires a symmetry change across the boundary of the RIQHE

state.

In order to gain insight into the physics of RIQHE, it is instructive to analyze the effect of strain on resistivity from the vantage point afforded by symmetry invariants. Finite conductivity is due to movement of charge defects, where an extra electron on a bubble (or a lack of one) can hop through the bubble lattice. We write down the expression for electric current in the ohmic approximation using a real space approach, $\mathbf{j} = \int \mathbf{r}(e\mathbf{E}\mathbf{r})f(\mathbf{r})d\mathbf{r}$, where \mathbf{E} is the electric field, \mathbf{r} is the electron coordinate operator, and $f(\mathbf{r})$ describes the distribution of charge and reflects the presence of strain and other symmetry factors. For this symmetry analysis it is sufficient to consider \mathbf{r} continuous; the results are the same as for consideration of hopping over discrete lattice sites. Resistivity ρ_{ii} is defined by the spatial average $\langle r_i^2 f(\mathbf{r}) \rangle$. The function $f(\mathbf{r})$ can be conveniently written as a product of symmetry invariants. The symmetry invariant $T_1 = (\varepsilon_{xx} - \varepsilon_{yy})(\mathbf{r}_x^2 - \mathbf{r}_y^2)$ describes electron hopping in an ideal lattice deformed by strain and motion of non-textured charge defects, as shown in Figs. 3(a,b). Anisotropy of $f(\mathbf{r}) \propto T_1$ is similar to the strain-induced anisotropy of the effective mass: the sign of corresponding β would be the same across all RIQHE regions in contrast to the experimental data. However, we discover that in the vicinity of charge defects bubbles change their shape from round to elongated, which results in the formation of non-trivial textures, Fig. 3c. We identify two possible textures: vortices and 2D hedgehogs described by functions $T_2^{(v)} = (\mathbf{a} \times \mathbf{r})_z^2$ and $T_2^{(h)} = (\mathbf{a} \cdot \mathbf{r})^2$, where vector \mathbf{a} is the elongation of a bubble. In the presence of bubble elongations, strain affects the system via the symmetry invariant $T_3 = (\varepsilon_{xx} - \varepsilon_{yy})(\mathbf{a}_x^2 - \mathbf{a}_y^2)$. Calculating the resistivity $\langle r_i^2 f(\mathbf{r}) \rangle$ by averaging over \mathbf{a} for $f^{(h)}(\mathbf{r}) \propto T_2^{(h)}T_3$ and $f^{(v)}(\mathbf{r}) \propto T_2^{(v)}T_3$, we arrive to the opposite sign of β for vortices and hedgehogs. Below we show that a microscopic calculation of resistivity shows the sign change as seen in experiment. Vortex topological excitations dominate on one side of RIQHE, while hedgehogs dominate on the other side, which results in the symmetry change across the RIQHE necessary for the change of the sign of β . We note here that from the vantage point afforded by symmetry $\varepsilon_{xx} - \varepsilon_{yy}$ behaves exactly like an expression $H_x^2 - H_y^2$ in the presence of tilted magnetic field, where H_x and H_y are the in-plane components of the field. Therefore it is possible that experiments in tilted field will also reveal opposite effects on resistivity due to vortices and hedgehogs.

To describe microscopic properties of the the system we use the real space approach of “interacting guiding centers” proposed by Ettouhami[20]. Throughout the rest of the paper distances are expressed in units of magnetic length λ , wavevectors in units of $1/\lambda$ and energies in units of $e^2/\kappa\lambda$, where κ is the background dielectric constant. In this approach, the Hartree-Fock (HF) Hamiltonian is the sum of effective interactions between guiding centers: $H_{\text{HF}} = 1/2(\sum_{i \neq j} U(\mathbf{R}_{ij}) + \sum_i U(0))$ where i and j labels the nodes of triangular lattice, \mathbf{R}_i is the coordinate of the bubble i , $\mathbf{R}_{ij} = \mathbf{R}_i - \mathbf{R}_j$. An effective interaction between bubbles i and j is given by

$$U(\mathbf{R}_{ij}) = \int \frac{d^2\mathbf{q}}{(2\pi)^2} \rho_i^*(\mathbf{q}) [V_{\text{H}}(\mathbf{q}) - V_{\text{F}}(\mathbf{q})] \rho_j(\mathbf{q}) \exp(i\mathbf{q} \cdot \mathbf{R}_{ij}), \quad (1)$$

where ρ_i represents the density of the bubble located at site i projected on the uppermost Landau Level. The Hartree potential and exchange potentials are, respectively [22], $V_{\text{H}}(\mathbf{q}) = \frac{2\pi}{q} e^{-q^2/2} [L_n(q^2/2)]^2$, and $V_{\text{F}}(\mathbf{q}) = 2\pi \int \frac{d^2\mathbf{q}'}{(2\pi)^2} V_{\text{H}}(\mathbf{q}) e^{-i(\mathbf{q} \times \mathbf{q}') \cdot \hat{z}}$, where L_n is the n^{th} Laguerre polynomial. To describe the experimental data we concentrate on a two-electron bubble crystal and its excitations. The ground state of an ideal bubble crystal at zero temperature is characterized by round bubbles. Calculated energies of isolated $1\bar{e}$ and $3\bar{e}$ defect in a

crystal of round bubbles taking into account displacements of lattice bubbles due to defect are plotted in Fig. 4 with dashed lines. Apart from the symmetry of these defects being inconsistent with the strain dependence of resistivity, their activation energies are in the range of several Kelvin and, thus, cannot explain high conductivity measured around 100 mK.

The presence of charged defects induces elongation of bubbles in the vicinity of defects. The wavefunction of an elongated two-electron bubble with guiding centers separated by $2\mathbf{a}$ is:

$$\Psi_{\xi,\mathbf{a}}(\mathbf{r}_1, \mathbf{r}_2) = \alpha (\psi_{\mathbf{a}}(\mathbf{r}_1, \mathbf{r}_2) + \xi \psi_{-\mathbf{a}}(\mathbf{r}_1, \mathbf{r}_2)) \quad (2)$$

where α is the normalization coefficient,

$$\psi_{\mathbf{a}}(\mathbf{r}_1, \mathbf{r}_2) = [u_{-2}(\mathbf{r}_1 + \mathbf{a})u_{-1}(\mathbf{r}_2 - \mathbf{a})e^{i(\mathbf{r}_1 - \mathbf{r}_2) \times \mathbf{a}/2} - u_{-1}(\mathbf{r}_1 - \mathbf{a})u_{-2}(\mathbf{r}_2 + \mathbf{a})e^{i(\mathbf{r}_2 - \mathbf{r}_1) \times \mathbf{a}/2}],$$

u_{-2} and u_{-1} are single-electron wavefunctions on the 3rd Landau level (3LL) in the symmetric gauge with angular momentum projections $m = -2$ and $m = -1$ [23]. This is a trial variational wavefunction, similar in spirit to the one proposed by Fogler and Koulikov for round bubbles[17]. The wavefunction (2) reflects both the magnitude and orientation of bubble elongation.

Expressions for the electron density of an elongated bubble projected on the 3LL, $\rho_{\xi,\mathbf{a}}(\mathbf{q})$, and interaction energy between of elongated bubbles, $U_2(\mathbf{R}_{i,j})$, are presented in the Supplemental Information. Besides $U_2(\mathbf{R}_{i,j})$, the total energy includes contributions from charged defects. The wavefunction of a $1\bar{e}$ bubble is $u_{-2}(\mathbf{r})$ and has round shape. The wavefunction of a $3\bar{e}$ bubble is a Slater determinant made of u_{-2} , u_{-1} , and $u_{m=0}$. Exact structure and shape of these defects can be determined by minimizing the cohesive energy, however, energetics and electron transport are primarily determined by elongations of the crystalline two-electron bubbles. Thus, the detailed structure of the $3\bar{e}$ bubble is not essential and we model it as having all three guiding centers on top of each other. We now calculate interactions of a single charge defect at a site k with $2\bar{e}$ bubbles. It is convenient to express these interactions in terms of elongations \mathbf{a}_i and effective dipole moments $\boldsymbol{\mu}_i(\mathbf{a}_i)$, which represent rotated and rescaled \mathbf{a}_i . Retaining terms up to R_{ik}^{-3} we arrive to elongation-dependent part of asymptotic expansion of energy:

$$H^\pm = \sum_{i \neq k} \left[\mp \left[\frac{\boldsymbol{\mu}_i \cdot \hat{\mathbf{R}}_{ik}}{R_{ik}^2} + \frac{v_i}{2R_{ik}^3} \cos(2\varphi_i) \right] + U_f^\pm(i) \right] + \frac{1}{2} \sum_{i \neq j} \frac{\boldsymbol{\mu}_i \cdot \boldsymbol{\mu}_j - 3(\boldsymbol{\mu}_i \cdot \hat{\mathbf{R}}_{ij})(\boldsymbol{\mu}_j \cdot \hat{\mathbf{R}}_{ij})}{R_{ij}^3}, \quad (3)$$

where (+) and (−) signs correspond to $1\bar{e}$ and $3\bar{e}$ defects, $\hat{\mathbf{R}}_{ij} = \mathbf{R}_{ij}/R_{ij}$ and φ_i is the angle between \mathbf{a}_i and \mathbf{R}_i . The first three terms of Eq. (3) are contributions to energy at the site i due to the presence of the defect, and the fourth term is an elongation-dependent interaction between two sites i and j . Explicit expressions for $\boldsymbol{\mu}_i$, v_i , and $U_f^\pm(i)$, are given in Supplementary Information.

The ground state of the bubble system in the presence of elongations caused by a defect is obtained by minimizing the energy (3). For $1\bar{e}$ defects the energy minimum corresponds to $\varphi_i = 0, \pi$, which we call vortices and anti-vortices correspondingly, and for $3\bar{e}$ defect the energy minimum occurs at $\varphi_i = \pi/2, 3\pi/2$, which we will call hedgehogs and anti-hedgehogs (although these are 2D objects). The two chiralities of vortex and hedgehog

textures are almost degenerate and the difference can be ignored for experimentally relevant temperatures. The activation energies of the defects in the presence of elongations of lattice bubbles are shown by solid lines in Fig. 4b. The resulting energies are 10 times smaller than excitation energies for charge defects in the absence of textures, and are consistent with experimentally studied range of temperatures. Density profiles of vortex and hedgehog defects are plotted in Fig. 4a. The term which describes the interaction of elongated bubbles is essentially given by the XY-model for which these textures are topological excitations. Minimization of energy provides the magnitudes of elongations a_i ($a_i \sim \lambda$) and wavefunction mixing parameters ξ_i , which are given in the Supplemental Information. An important result of minimization is that textured deformation of the bubble crystal is extended over a finite distance $L \sim 10w$ from the charge defect, where $w \sim 8\lambda$ is the lattice constant of the bubble crystal. As distance R_{ik} from the center of the charge defect increases, bubble elongation a_i decreases and the parameter ξ_i in the wavefunction (2) evolves towards -1. At $R_{ik} \sim L$ the symmetric wavefunction ($\xi_i \sim 1$) becomes energetically favorable, and round bubbles ($a_i = 0$) are recovered for $R_{ik} > L$.

At very low temperatures the density of defects is low, defect separation is $> L$, textures from different defects do not overlap, and charged defects interact via Coulomb interaction. Consider first minimization of interaction energy for defects of the same sign. Such defects form a superlattice superimposed on the bubble crystal, somewhat similar to the Wigner[3] or Abrikosov[12] lattice. Defects with opposite charges cannot easily approach and annihilate each other due to the difference in the symmetry of their textures, and we expect a texture crystal to form even when charge defects of both signs are present. When temperature increases or filling factor is shifted from the center of the RIQHE state, the density of defects increases, see Fig. 4. When the defect separation becomes $< 2L$ textures of neighboring defects start to overlap and energy (3) includes interaction between elongated bubbles belonging to different defects. This interaction is described by the XY model. In order to calculate energy caused by such interaction, we take the lower bound on the "exchange constant" J , which is the $\boldsymbol{\mu}_i \cdot \boldsymbol{\mu}_j$ term in (3). We assume that J is defined by a characteristic magnitude of elongations $a \sim \lambda$ in the region where topological excitations overlap, which sets the lower bound to $J \sim e^2 a^2 / \kappa L^3$. The entropy of topological excitations is given then by[24]

$$E = (\pi J - 2T) \ln(\mathcal{L}/w), \quad (4)$$

where \mathcal{L} is the size of the system and the core of topological excitations is taken to be of the order of the bubble crystal lattice constant w . Such a system must exhibit the Berezinski-Kosterlitz-Thouless (BKT) transition [10, 11] at $T_{KT} = \pi J/2$. However, the thermodynamic transition in the RIQHE regime differs from a conventional BKT transition, e.g., as discussed in [25], due to the finite size of topological defects L . At low densities there is no overlap between neighboring defects, and thus, the system cannot undergo the BKT transition. The temperature T_L , at which textures from neighboring defects begin to overlap, corresponding to defect density $1/(\pi L^2)$, is much higher than the estimated $T_{KT} \approx 5$ mK. Thus, T_{KT} itself is not observed experimentally. The unbinding of topological defects at T_L required to avoid the divergence of logarithmic interactions in (S41) constitutes *melting of the defect rather than the bubble crystal*. We plot T_L in Fig. 4c and over the $R_{xx}(T, B)$ data in Fig. 2. The calculated T_L describes the measured temperature of the insulating-to-conducting transition remarkably well. Following Thouless [26, 27] we estimate that melting of an ideal bubble crystal due to dislocations takes place at $T_m \approx 400$ mK $> T_L$. Thus we expect that topological defects continue to exist within some temperature range above T_L .

We conclude that the presence of topologically non-trivial textures around charge defects is responsible for the observed strain dependence of resistivity.

We now address the microscopic mechanism of strain response of the resistivity tensor, and how it depends on the symmetry of topological defects. Effects of strain $\varepsilon_{xx} = -\varepsilon_{yy} = \varepsilon$ is added to the model similarly to the case of the stripe phase[15] using a deformed coordinate system $x \rightarrow x(1 + \varepsilon)$, $y \rightarrow y(1 - \varepsilon)$. In this coordinate system the lattice is identical to the unstrained one, but the interaction potential becomes anisotropic. The linear in strain contribution to the Hamiltonian in a real space representation can be written as $H_\varepsilon = -\varepsilon \tilde{U}_f^\varepsilon(a) \cos[2(\phi_i - \theta_{ik})]$, where $(\phi_i - \theta_{ik})$ and θ_{ik} are polar angles of \mathbf{a}_i and \mathbf{R}_{ik} , and $\tilde{U}_f^\varepsilon(a)$ is defined in the supplement. Note that $\varepsilon a^2 \cos[2(\phi_i - \theta_{ik})]$ is precisely the T_2 invariant in our symmetry argument. After minimizing the total energy we find that strain leads to small rotations of elongated bubbles

$$\delta\phi_i = \varepsilon\gamma_i \sin[2(\phi_i - \theta_{ik})] = \pm\varepsilon\gamma_i \sin(2\theta_{ik}), \quad (5)$$

where the positive sign corresponds to vortex ($\phi_i = 0, \pi$) and negative to hedgehog ($\phi_i = \pi/2, 3\pi/2$) textures, $\gamma_i = \frac{1}{\beta_i} U_f^\varepsilon$. Effect of strain on defect textures is sketched in Fig. 4.

A strain dependent contribution to conductivity arises from re-adjustment of textures and rotation of elongated $2\bar{e}$ bubbles by an angle $\Delta\theta_i = (\theta_{ik} - \theta_{ik'}) + [\delta\phi_i(\theta_{ik}) - \delta\phi_i(\theta_{ik'})] = \Delta\theta_i^a + \Delta\theta_i^\varepsilon$ when defect charge hops from site k to k' . Overlap between the initial and the final state of the bubbles is $p(\Delta\theta_i) = \langle \Psi_{ik}^* | \Psi_{ik'} \rangle = 1 - \alpha(a_i)(\Delta\theta_i)^2$, and the conductivity

$$\sigma_s^{(h,v)} \propto \prod_i p(\Delta\theta_i), \quad (6)$$

where the product includes contributions from all bubbles that rotate or change shape during the charge hopping event. Rotation of elongated bubbles $\Delta\theta_i^a = (w/R_{ik}) \sin[\theta_{ik} + (1+s)\frac{\pi}{4}]$ leads to a strain-independent contribution to conductivity when defect shifts by distance w in the \hat{x} ($s = 1$) or \hat{y} ($s = -1$) direction. A strain-dependent rotation $\Delta\theta_i^\varepsilon = \mp\gamma_i \cos(2\theta_{ik})\Delta\theta_i^a$ has different sign for hedgehogs (+) and vortices (-).

Strain-induced anisotropy of resistivity tensor has different sign depending on whether current is carried by $1\bar{e}$ or $3\bar{e}$ defects in a $2\bar{e}$ bubble crystal. The ratio $\rho^{(v)}/\rho^{(h)}$ is calculated using (6) and is plotted in Fig. 5 as a function of strain. A corresponding ratio of resistances $R^{(v)}/R^{(h)}$ is further amplified by the van der Pauw geometry [28]. Experimentally measured strain dependence of magnetoresistance in the vicinity of RIQHE states on the 2LL and 3LL is plotted in Fig. 5c. For each state the ratio R^R/R^L is extracted, where R^L and R^R are resistances on the low- ν (L) and high- ν (R) sides of the RIQHE state. Good quantitative agreement between $R^{(v)}/R^{(h)}$ and R^R/R^L for the B_1 state strengthen our conclusion that $1\bar{e}$ (hedgehog) charge excitations dominate on the low- ν side of B_1 , while $3\bar{e}$ (vortex) excitations dominate on the high- ν side. Thus our theory explains both the symmetry and unusually large magnitude of strain's effect on resistivity, in addition to identifying the temperatures of the observed metal-insulator transitions. Opposite strain dependence of B_2 underscores that the system largely possesses an electron-hole symmetry. Surprisingly, strain dependence measured for the I_1 and I_3 states on the 2LL is similar to the strain dependence of the B_1 and B_2 states on the 3LL. This observation lead us to suggest that RIQHE states observed on the 2LL originate from a crystal of defects in a $2\bar{e}$ bubble crystal interrupted by fractional quantum Hall effect states. We note that despite the fact that Hartree-Fock approach loses its predictive power for electron interactions on Landau levels with lowest indices, the

similarity of strain dependence of resistivity on the 2LL and 3LL suggests that change of symmetry of topological textures with magnetic field plays an important role in the physics of electrons even on the 2LL.

Methods Summary

Samples are fabricated from modulation-doped 30-nm wide AlGaAs/GaAs/AlGaAs quantum wells grown on (001) GaAs by molecular beam epitaxy. Devices are cleaved along (110) crystallographic direction. Eight Ohmic contacts are formed along the edge of a sample by annealing InSn alloy at 420°C for 3 min. Devices attached to a multilayered piezoelectric transducer with epoxy with either (110) (yy) or ($\bar{1}\bar{1}0$) (xx) aligned with the transducer polling direction. A thin layer of metallized plastic foil is inserted between the sample and the transducer, the foil is grounded during the experiments in order to screen possible non-uniform electric fields. A shear strain induced in the sample $\varepsilon = \varepsilon_{xx} - \varepsilon_{yy} \approx 2.5 \cdot 10^{-7} V_p$, where V_p is the voltage on the transducer and $\varepsilon_{xx} \approx -2\varepsilon_{yy}$ for the (xx) poling direction. The actual strain $\varepsilon_{tot} = \varepsilon_{th} + \varepsilon$, where thermally-induced strain ε_{th} depends on the cooldown conditions. The 2D electron gas is illuminated with a red LED at 10 K for 20 min. Several samples from two different wafers with mobility $\sim 1 \cdot 10^7$ cm²/Vs and density $2 - 3 \cdot 10^{11}$ cm⁻² at 0.3 K were investigated, all show similar results. Measurements are performed in a van der Paw geometry using low frequency (17 Hz) lock-in technique with excitation current $I_{ac} = 10$ nA.

Acknowledgements Research was partially supported by the U.S. Department of Energy, Office of Basic Energy Sciences, Division of Materials Sciences and Engineering under Awards DE-SC0008630 (L.P.R.), DE-SC0010544 (Y.L-G), DE-SC0006671 (G.S. and M.M.).

Authors contribution L.P.R. conceived and designed the experiments, T.L. performed measurements. G.S. and Y.L-G proposed explanation of the experimental results and put forward the theory. J.W. and M. J. M. designed and grew wafers for the experiments, and G.C. provided data from unstrained samples. Y.L-G and L.P.R. and M. J. M. contributed to writing the paper.

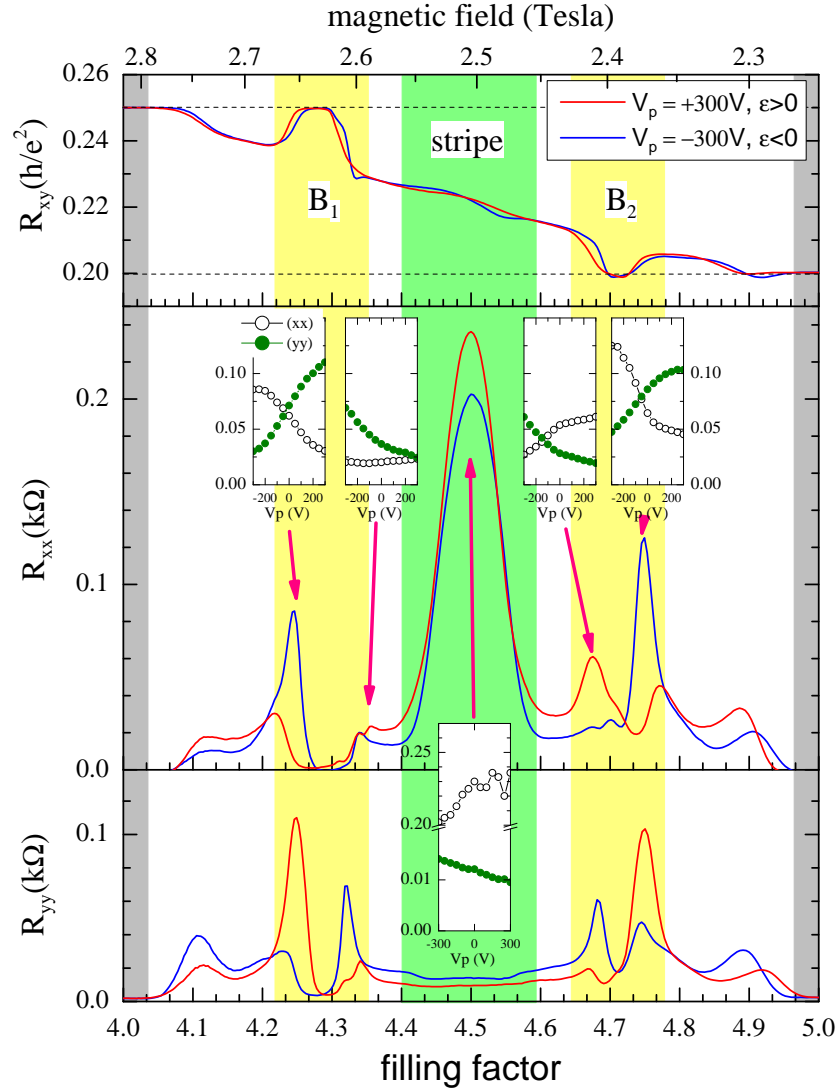


FIG. 1. **Strain dependence of re-entrant QHE phases near filling factor $\nu = 9/2$.** Colored regions mark IQHE states (grey), RIQHE phases B_1 , B_2 (yellow) and the stripe phase (green). In the inserts resistance of the peaks marked by arrows are plotted as a function of strain for R_{xx} (blue) & R_{yy} (red). Strain dependence of the stripe phase at $\nu = 9/2$ is also shown, note the break in the vertical axis. The data is taken at 100 mK.

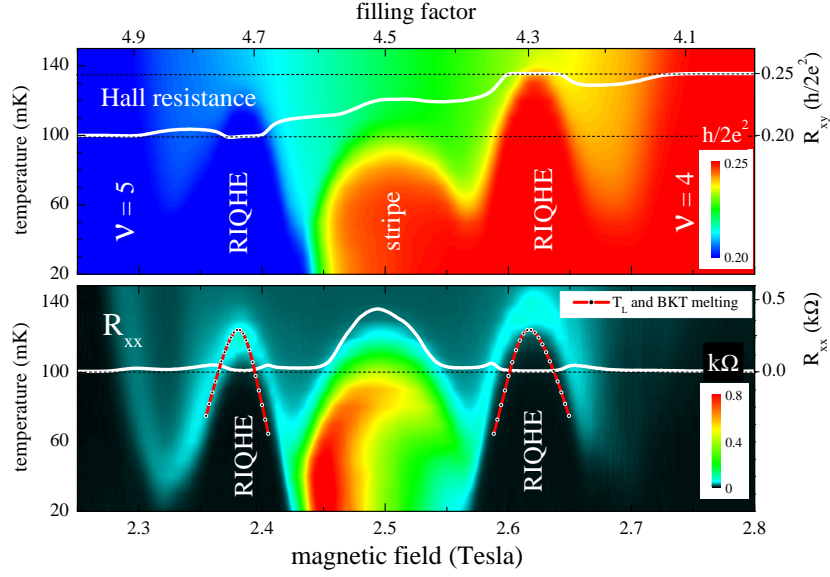


FIG. 2. **Experimental phase diagram of melting transitions.** Calculated phase boundary $T_L(B)$, where topological defects start to overlap resulting in melting of the defect crystal, is plotted on top of the experimentally measured temperature dependence of R_{xx} and coincides with the sharp increase of conductance at the boundary of isolating and conducting phases. Color scales for R_{xy} is in $h/2e^2$ and for R_{xx} in $k\Omega$, the white scans are measured at $T = 100$ mK.

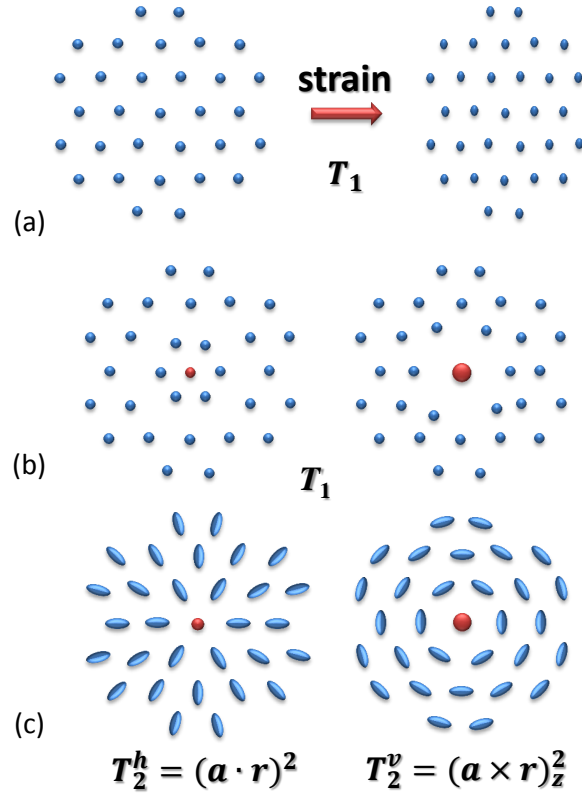


FIG. 3. **Symmetry of bubble crystal and defects.** (a) Uniaxial strain induces anisotropy of the effective mass and uniaxial deformation of bubble crystal which is described by the symmetry invariant T_1 . (b) Density of bubbles alters in the vicinity of charged defects, but in the absence of textures, strain response is described by the same T_1 invariant. (c) functions $T_2^v = (\mathbf{a} \times \mathbf{r})_z^2$ and $T_2^h = (\mathbf{a} \cdot \mathbf{r})^2$ give charge distributions different for vortex and hedgehog patterns, where \mathbf{a} characterizes bubble elongation and \mathbf{r} - distance between the center of the defect and elongated bubbles.

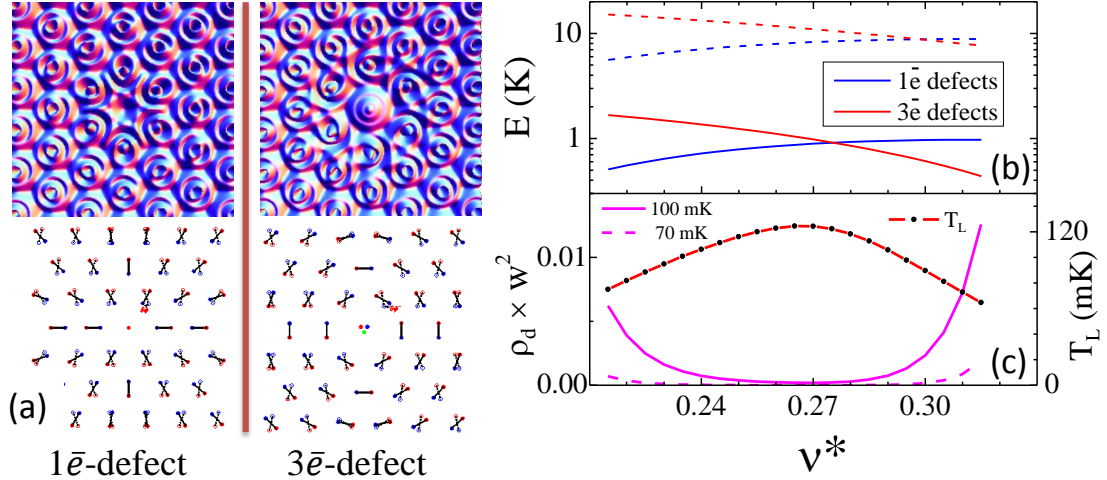


FIG. 4. **One- and three-electron defects in a two-electron bubble crystal.** (a) Electron density profile in the vicinity of defects. The corresponding textures of bubble elongations are shown schematically at the bottom. Dotted lines indicate rotations of elongated bubbles under horizontal compressive and vertical tensile strain. (b) Activation energy for an isolated defect calculated as a function of the filling factor of the top-most LL ν^* for optimal elongations (solid lines) and for round bubbles (dashed lines). Note that textures of elongated bubbles significantly reduce activation energies for defects. (c) Density of defects ρ_d calculated for 70 mK and 100 mK. Transition temperature T_L corresponds to the condition $\rho_d(T_L, B) = 1/(\pi L^2)$.

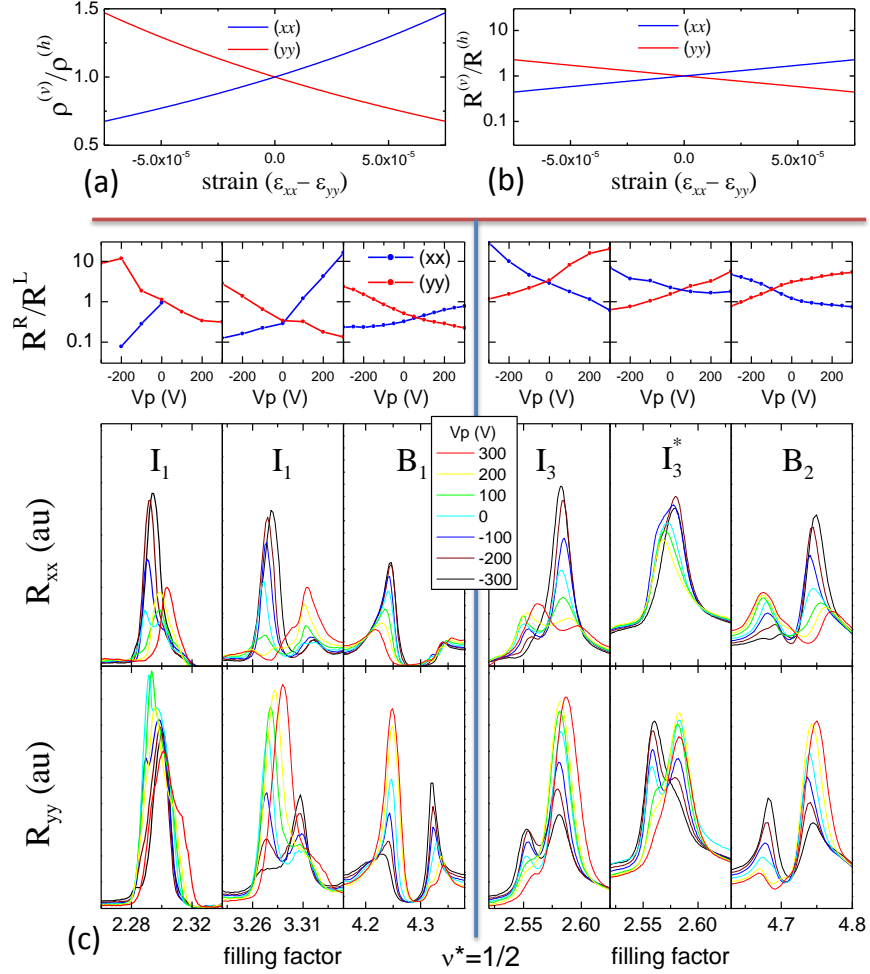


FIG. 5. **Strain dependence of resistivity in the presence of topological defects.** (a) Ratio of resistivities for the transport dominated by vortex $\rho^{(v)}$ and hedgehog $\rho^{(h)}$ charge defects is calculated using Eq. 6 and the corresponding ratio of resistances is plotted for a square van der Pauw geometry [28] in (b). (c) Magnetoresistance near RIQHE states on 2nd & 3rd LLs measured with different strains (voltages on the piezo transducer V_p). Heights of the resistance peaks R^L and R^R on the left and right sides of RIQHE states are extracted from two peak Lorentzian fits, the corresponding ratio R_R/R_L is plotted at the top of each data set.

-
- [1] K. v. Klitzing, G. Dorda, and M. Pepper, “New method for high-accuracy determination of the fine-structure constant based on quantized Hall resistance,” *Phys. Rev. Lett.* **45**, 494–497 (1980).
- [2] D. C. Tsui, H. L. Störmer, and A. C. Gossard, “Two-dimensional magnetotransport in the extreme quantum limit,” *Phys. Rev. Lett.* **48**, 1559 (1982).
- [3] E. Wigner, “On the interaction of electrons in metals,” *Phys. Rev.* **46**, 1002–1011 (1934).
- [4] G. Moore and N. Read, “Nonabelions in the fractional quantum Hall effect,” *Nuc. Phys. B* **360**, 362–396 (1991).
- [5] A. A. Koulakov, M. M. Fogler, and B. I. Shklovskii, “Charge density wave in two-dimensional electron liquid in weak magnetic field,” *Phys. Rev. Lett.* **76**, 499 – 502 (1996).
- [6] R. R. Du, D. C. Tsui, H. L. Stormer, L. N. Pfeiffer, K. W. Baldwin, and K. W. West, “Strongly anisotropic transport in higher two-dimensional Landau levels,” *Solid State Commun.* **109**, 389 – 94 (1999).
- [7] M. P. Lilly, K. B. Cooper, J. P. Eisenstein, L. N. Pfeiffer, and K. W. West, “Evidence for an anisotropic state of two-dimensional electrons in high Landau levels,” *Phys. Rev. Lett.* **82**, 394–397 (1999).
- [8] J.P. Eisenstein, M.P. Lilly, K.B. Cooper, L.N. Pfeiffer, and K.W. West, “New collective states of 2D electrons in high Landau levels,” *Physica E: Low-dimensional Systems and Nanostructures* **9**, 1 – 8 (2001).
- [9] J.P. Eisenstein, “Two-dimensional electrons in excited Landau levels: evidence for new collective states,” *Solid State Communications* **117**, 123 – 131 (2001).
- [10] V.L. Berezinskii, “Destruction of long-range order in one-dimensional and 2-dimansional systems possessing a continuous symmetry group - II. Quantum systems.” *Sov. Phys. JETP* **34**, 610–616 (1972).
- [11] J M Kosterlitz and D J Thouless, “Ordering, metastability and phase transitions in two-dimensional systems,” *Journal of Physics C: Solid State Physics* **6**, 1181–1203 (1973).
- [12] A.A. Abrikosov, “On the magnetic properties of superconductors of the second group,” *Soviet Physics JETP-USSR* **5**, 1174–1183 (1957).
- [13] David J. Gross and Frank Wilczek, “Ultraviolet behavior of non-abelian gauge theories,” *Phys. Rev. Lett.* **30**, 1343–1346 (1973).
- [14] N. Deng, A. Kumar, M. J. Manfra, L. N. Pfeiffer, K. W. West, and G. A. Csáthy, “Collective nature of the reentrant integer quantum Hall states in the second Landau level,” *Phys. Rev. Lett.* **108**, 086803 (2012).
- [15] Sunanda P. Koduvayur, Yuli Lyanda-Geller, Sergei Khlebnikov, Gabor Csathy, Michael J. Manfra, Loren N. Pfeiffer, Kenneth W. West, and Leonid P. Rokhinson, “Effect of strain on stripe phases in the quantum Hall regime,” *Phys. Rev. Lett.* **106**, 016804 (2011).
- [16] M. M. Fogler, A. A. Koulakov, and B. I. Shklovskii, “Ground state of a two-dimensional electron liquid in a weak magnetic field,” *Phys. Rev. B* **54**, 1853 – 71 (1996).
- [17] M. M. Fogler and A. A. Koulakov, “Laughlin liquid to charge-density-wave transition at high Landau levels,” *Phys. Rev. B* **55**, 9326–9329 (1997).
- [18] M. O. Goerbig, P. Lederer, and C. Morais Smith, “Microscopic theory of the reentrant integer quantum Hall effect in the first and second excited Landau levels,” *Phys. Rev. B* **68**, 241302 (2003).

- [19] R. Côté, C. B. Doiron, J. Bourassa, and H. A. Fertig, “Dynamics of electrons in quantum Hall bubble phases,” *Phys. Rev. B* **68**, 155327 (2003).
- [20] A. M. Ettouhami, F. D. Klironomos, and Alan T. Dorsey, “Static and dynamic properties of crystalline phases of two-dimensional electrons in a strong magnetic field,” *Phys. Rev. B* **73**, 165324 (2006).
- [21] M. M. Fogler, *High Magnetic Fields: Applications in Condensed Matter Physics and Spectroscopy*, edited by C. Berthier, L.P Levy, and G. Martinez, *Lect. Notes Phys.*, Vol. 595 (Springer, Berlin, 2002) pp. 98–138.
- [22] I. L. Aleiner and L. I. Glazman, “Two-dimensional electron liquid in a weak magnetic field,” *Phys. Rev. B* **52**, 11296–11312 (1995).
- [23] G. Giuliani and G. Vignale, *Quantum theory of the electron liquid* (Cambridge University Press, 2005).
- [24] P. M. Chaikin and T. C. Lubensky, *Principles of Condensed Matter Physics* (Cambridge University Press, 2000).
- [25] Petter Minnhagen, “The two-dimensional Coulomb gas, vortex unbinding, and superfluid-superconducting films,” *Rev. Mod. Phys.* **59**, 1001–1066 (1987).
- [26] D. J. Thouless, “Melting of a two-dimensional wigner lattice,” *Journal of Physics C: Solid State Physics* **11**, L189 (1978).
- [27] D.S. Fisher, B.I. Halperin, and R. Morf, “Defects in two-dimensional electron solid and implications for melting,” *Phys. Rev. B* **20**, 4692–4712 (1979).
- [28] Steven H. Simon, “Comment on “evidence for an anisotropic state of two-dimensional electrons in high landau levels”,” *Phys. Rev. Lett.* **83**, 4223–4223 (1999).

Supplementary Information

NEW TOPOLOGICAL EXCITATIONS AND MELTING TRANSITIONS IN QUANTUM HALL SYSTEMS

Tzu-ging Lin, George Simion, John D. Watson, Michael J. Manfra, Gabor A. Csathy, Yuli Lyanda-Geller, and Leonid P. Rokhinson

I. THEORY OF TOPOLOGICAL EXCITATIONS IN THE QUANTUM HALL REGIME

The purpose of the theory section of the supplement is the detailed demonstration of how topological defects of different symmetry arise in the electron bubble crystal, how they are influenced by external strain, and how they contribute to transport properties of the system.

The HF Hamiltonian of partially filled n^{th} Landau level is given by [22]:

$$H_{\text{HF}} = \frac{1}{2} \int \frac{d^2\mathbf{q}}{(2\pi)^2} [V_{\text{H}}(\mathbf{q}) - V_{\text{F}}(\mathbf{q})] |\rho(\mathbf{q})|^2, \quad (\text{S1})$$

where $\rho(\mathbf{q})$ is the projected electronic density onto the uppermost LL and the Hartree potential and exchange potentials are, respectively:

$$V_{\text{H}}(\mathbf{q}) = \frac{2\pi}{q} e^{-q^2/2} [L_n(q^2/2)]^2, \quad (\text{S2})$$

$$V_{\text{F}}(\mathbf{q}) = 2\pi \int \frac{d^2\mathbf{q}'}{(2\pi)^2} V_{\text{H}}(\mathbf{q}') e^{-i(\mathbf{q} \times \mathbf{q}') \cdot \hat{z}}, \quad (\text{S3})$$

where L_n is the n^{th} Laguerre polynomial.

A charge density wave state was proposed as the ground state for 2D systems in the lowest Landau level [29] even prior discovery of the quantum Hall effect. This prediction appeared not to describe the lowest Landau level, but is relevant to the two-dimensional electron liquid in higher Landau levels where phases compete [21]. Hartree-Fock (HF) studies suggest bubble or stripe phases as possible ground states [5, 17–20]. In the bubble phase guiding centers of electron cyclotron orbits form a triangular lattice. A Wigner crystal, a triangular lattice with one electron per lattice cell, is energetically favorable at small effective filling factors $\nu^* = \nu - n_f < 0.2$, where n_f is the number of filled Landau levels and ν is the filling factor. For higher effective filling factors bubble phases with more than one electron per site are the ground state. HF calculations [17–20] indicate the presence of bubble phases with $M \leq n + 1$ electrons per bubble. The conventional picture of bubble phases is that crystals with integer number of electrons per bubble exist in certain range of filling factors, with lattice constant dependent on filling factor, and first order phase transitions occur between crystals with different number of electrons per bubble. Density matrix renormalization group method suggests a limit on the size of bubbles $M \leq n$ [30, 31]. For effective filling factors close to 0.5, the stripe phase occurs.

Considering bubble phases, it is convenient to express the HF Hamiltonian as the sum of effective interactions between the guiding centers: $H_{\text{HF}} = 1/2 [\sum_{i \neq j} U(\mathbf{R}_{ij}) + \sum_i U(0)]$ where i and j labels the nodes of the triangular lattice. The effective interaction U is given by:

$$U(\mathbf{R}_{ij}) = \int \frac{d^2\mathbf{q}}{(2\pi)^2} \rho_i^*(\mathbf{q}) [V_{\text{H}}(\mathbf{q}) - V_{\text{F}}(\mathbf{q})] \rho_j(\mathbf{q}) \exp(i\mathbf{q} \cdot \mathbf{R}_{ij}), \quad (\text{S4})$$

where ρ_i represents the projected density of the bubble located at site i . We surmise that Hartree-Fock approach captures physics of the quantum Hall systems even at low n , particularly on the 3rd LL ($n = 2$) and 2nd LL ($n = 1$) [18–20].

We now seek the many-body wavefunction in the range of electron densities favorable for existence of two-electron bubbles. Experimental data leads us to consideration of one and three-electron bubble defects in the two-electron bubble crystal. Indeed, our experiment shows a conducting state above a certain temperature. In the absence of defects, the only possible conduction mechanism comes from melting of the bubble crystal and transition to a bubble liquid. However, in such a liquid, effect of strain on resistivity would be similar to the effect on resistivity caused by anisotropy of the effective mass in the presence of strain, which has the same sign throughout the range of filling factors corresponding to reentrant integer quantum Hall effect. Thus, we explore the possibility that novel defects in the two-electron bubble lattice might be favorable in the range of filling factors close the reentrant integer quantum Hall effect and are responsible for the results seen in strain experiments.

We theoretically demonstrate that it is energetically favorable for crystalline two-electron bubbles to change their shape and to become elongated. We will begin by considering how much energy it costs to create a defect in a bubble crystal, when crystalline bubbles continue to be arranged in a lattice. Next, we will assume the shape of the crystalline bubbles to be round, but will allow their positions to re-adjust, lowering the activation energy of the defect. We then will compute the activation energy for defects taking into account elongation of crystalline bubbles.

Consider a system of 2 electron crystalline bubbles with a microscopic number N_d of infinitely separated defects that are bubbles with $2 - \sigma_d$ electrons ($\sigma_d = \pm 1$). Considering the electron system at a fixed filling factor, we keep the total number of electrons $2N$.

The ground state is the triangular lattice of N 2-electron bubble electrons, with lattice constant w . When defects are present, the total number of bubbles has to change to $N + N_d\sigma_d/2$, as we keep the total number of electrons the same. Assuming all bubbles to be still arranged in a triangular lattice, we find that the change in lattice constant is $\delta w = -w\sigma_d N_d/(4N)$. Then the energy of the lattice with defects is:

$$\frac{1}{2}N \left[1 - \left(1 - \frac{\sigma_d}{2} \right) \frac{N_d}{N} \right] \epsilon_2^{(w+\delta w)} + N_d \epsilon_d^{(w+\delta w)}, \quad (\text{S5})$$

where ϵ_2^w is the energy required to add one 2-electron bubble in the bubble crystal with lattice constant w , ϵ_d^w is the energy of a defect embedded in an otherwise pristine system with lattice constant w .

From Eq. (S4), ϵ_2^w can be expressed as

$$\epsilon_2 = \sum_k \zeta_k a_k^{(2)}/w^{2k+1} + \tilde{U}(0), \quad (\text{S6})$$

where $\tilde{U}(0) = U(0)/2 = 833\sqrt{\pi}/2048$ is the formation energy, $a_0 = 4$, $a_1 = 14$, $a_2 = 765/4$. Similarly, the interaction between the defect and two-electron bubbles is $U_d = \sum_k \sum_k b_k^{(d)}/r^{2k+1}$, making $\epsilon_d = \sum_k \zeta_k b_k^{(d)}/w^{2k+1} + u_d$, where the formation energy of a one-electron bubble defect is $u_1 = 0$ while for the three-electron bubble defect $u_3 = 77463\sqrt{\pi}/65536$. For one electron defect we find $b_0(1) = 2$, $b_1(1) = 13/2$, $b_2(1) = 117/2$, and for three electron defect $b_0(3) = 6$, $b_1(3) = 45/2$ and $b_2(3) = 531/2$. The parameters ζ are $\zeta_0 = -4.2$, $\zeta_1 = 11.03$ and $\zeta_2 = 6.76$.

Using these expressions for ϵ_2 and ϵ_d we find the energy of N_d defects

$$N_d E_d = \frac{1}{2} N \left[1 - \left(1 - \frac{\sigma_d}{2} \right) \frac{N_d}{N} \right] \left(\epsilon_2(w) + \frac{\partial \epsilon_2}{\partial w} \delta w \right) + N_d \epsilon_d(w) - \frac{1}{2} N \epsilon_2(w) \quad (\text{S7})$$

The energy of one defect is:

$$E_d = -\frac{\sigma_d}{8} \frac{\partial \epsilon_2}{\partial w} w + \frac{\sigma_d - 2}{4} \epsilon_2 + \epsilon_d. \quad (\text{S8})$$

We now consider decrease in energy of the bubble lattice assuming the two-electron bubbles keep their round shape, but will allow positions of bubbles to deviate from triangular lattice. We approach this problem in the spirit of ideas of Fisher, Halperin and Morf [27]. Due to the presence of a defect with charge different from charge of surrounding bubbles, electron bubbles at lattice sites \mathbf{R}_i experience displacements $\mathbf{u}(\mathbf{R}_i)$ from their equilibrium positions. In the framework of elasticity theory, the energy associated with such displacements up to the second order in $\mathbf{u}(\mathbf{R}_i)$ is given by

$$E_d(\{\mathbf{u}_i\}) = \frac{1}{2} \sum_{i,j} \Pi_{\alpha\beta}(\mathbf{R}_i, \mathbf{R}_j) u_\alpha(\mathbf{R}_i) u_\beta(\mathbf{R}_j) - \sum_{i \neq i_0} \delta V_\alpha^1(\mathbf{R}_i) u_\alpha(\mathbf{R}_i) - \sum_{i \neq i_0} \delta V_{\alpha,\beta}^2(\mathbf{R}_i) u_\alpha(\mathbf{R}_i) u_\beta(\mathbf{R}_i) \quad (\text{S9})$$

where Π is the spring constant matrix,

$$\delta V_\alpha^1 = \frac{\partial}{\partial r_\alpha} [U_2(\mathbf{r}) - U_d(\mathbf{r})], \quad (\text{S10})$$

and

$$\delta V_{\alpha,\beta}^2 = \frac{1}{2} \frac{\partial^2}{\partial r_\alpha \partial r_\beta} [U_2(\mathbf{r}) - U_d(\mathbf{r})]. \quad (\text{S11})$$

Here the potential energy describing the bubble lattice U_2 is given by

$$U_2(\mathbf{R}_{ij}) = \frac{4}{R_{ij}} + \frac{14}{R_{ij}^3} + \frac{765}{4R_{ij}^5}, \quad (\text{S12})$$

the interaction energy of the two-electron bubble at site i with a one-electron defect at site k $U_{d=1}$ is given by

$$U_1(\mathbf{R}_{ik}) = \frac{2}{R_{ik}} + \frac{13}{2R_{ik}^3} + \frac{117}{2R_{ik}^5}, \quad (\text{S13})$$

the interaction energy of the two-electron bubble at site i with a three-electron defect at site k $U_{d=3}$ is given by

$$U_3(\mathbf{R}_{ik}) = \frac{6}{R_{ik}} + \frac{45}{2R_{ik}^3} + \frac{531}{2R_{ik}^5}. \quad (\text{S14})$$

Multipole terms in expansions (S12-S14) appear in magnetic field as a result of the shape of the electron wavefunction in the second Landau level. Because the bubble crystal lattice constant is about 8 magnetic lengths, we restrict these asymptotic expansions to three terms. Here and throughout the rest of the supplement we will express distances in units of magnetic length λ , wavevectors in units of $1/\lambda$ and energies in units of $e^2/\kappa\lambda$, where κ

is the background dielectric constant. The spring constant matrix is determined in terms of its Fourier-transform, which is related to Fourier-transforms of the potentials δV_α^1 and $\delta V_{\alpha,\beta}^2$ by

$$\delta V_{\alpha,\beta}^2(\mathbf{q}) = \frac{1}{2} \sum_{\gamma} V_{\gamma,\gamma} \delta_{\alpha\beta} + A_c \Pi_{\alpha\beta}^d \quad (\text{S15})$$

and

$$\delta V_\alpha^1(\mathbf{q}) = -iA_c \sum_{\gamma} \frac{\partial \Pi_{\gamma\gamma}^d}{\partial q_a}, \quad (\text{S16})$$

where A_c is the elementary cell area of the bubble lattice. Assuming a neutralizing background and writing the potential in the form

$$V(\mathbf{r}) = \sum_k \frac{a_k}{r^{2k+1}}, \quad (\text{S17})$$

we obtain an explicit expression for Π

$$A_c^2 \Pi_{\alpha\beta}(\mathbf{q}) = 2\pi \frac{q_\alpha q_\beta}{q} + \sum_k \frac{\Xi_k a_k}{w^{2k+1}} \left(q^2 \delta_{\alpha\beta} + \frac{4k+6}{2k-1} q_\alpha q_\beta \right), \quad (\text{S18})$$

where w is the lattice constant, and constants $\Xi_0 = 0.26$, $\Xi_1 = 2.07$ and $\Xi_2 = 6.34$. The change of energy of the lattice in terms of Fourier-transformed quantities is given by

$$E_d(\{\mathbf{u}_i\}) = \frac{1}{2} \int \frac{d\mathbf{q}}{4\pi^2} \Pi_{\alpha\beta}(\mathbf{q}) u_\alpha(\mathbf{q}) u_\beta(\mathbf{q}) - \int \frac{d\mathbf{q}}{4\pi^2} \delta V_\alpha^1(\mathbf{q}) u_\alpha(\mathbf{q}) - \int \frac{d\mathbf{q} d\mathbf{k}}{16\pi^4} \delta V_{\alpha,\beta}^2(\mathbf{q}-\mathbf{k}) u_\alpha(\mathbf{k}) u_\beta(-\mathbf{q}). \quad (\text{S19})$$

Minimization of this expression assuming

$$u_\alpha(\mathbf{q}) = \frac{q_\alpha}{q^2} f(1 + cq + dq^2) \quad (\text{S20})$$

gives a decrease in activation energy of the defects caused by displacements $\mathbf{u}(\mathbf{R}_i)$. In Fig.4b of the main paper, we plot the activation energy of one- and three-electron defects when the displacement of round crystalline bubbles is taken into account.

Further decrease in activation energy of the defects is caused by change of shape of bubbles from round to elongated. Until now bubbles were almost exclusively treated as entities with uniform charge density. Ettouhami et al.[32] suggested that the guiding centers in two-electron bubbles can be spatially separated in two dimensions. We find that if a proper superposition between wavefunctions of electrons in the same bubble is evaluated and the phase factors due to magnetic translations are taken into account, the energetically favorable ideal bubble crystal carries round shaped bubbles. What we also find, however, is that in the presence of charged defects, i.e. bubbles lacking one electron or with one extra electron, or in the presence of charged impurities, guiding centers of electrons within bubbles become spatially separated and two-electron bubbles become elongated. The wavefunction of a bubble with two guiding centers separated by $2a$ can be expressed as:

$$\Psi_{\xi,\mathbf{a}}(\mathbf{r}_1, \mathbf{r}_2) = \frac{\psi_{\mathbf{a}}(\mathbf{r}_1, \mathbf{r}_2) + \xi \psi_{-\mathbf{a}}(\mathbf{r}_1, \mathbf{r}_2)}{\sqrt{2(1 - 2e^{-2a^2} a^2)(1 + |\xi|^2) + 4(1 - 2a^2) e^{-2a^2} \Re(\xi)}}, \quad (\text{S21})$$

where

$$\Psi_{\mathbf{a}}(\mathbf{r}_1, \mathbf{r}_2) = u_{-2}(\mathbf{r}_1 + \mathbf{a})u_{-1}(\mathbf{r}_2 - \mathbf{a})e^{\frac{i}{2}(\mathbf{r}_1 - \mathbf{r}_2) \times \mathbf{a}} - u_{-1}(\mathbf{r}_1 - \mathbf{a})u_{-2}(\mathbf{r}_2 + \mathbf{a})e^{\frac{i}{2}(\mathbf{r}_2 - \mathbf{r}_1) \times \mathbf{a}}, \quad (\text{S22})$$

where u_{-2} and u_{-1} are the single electron wavefunction in third Landau level ($n = 2$) in the symmetric gauge [23]. This is a trial wavefunction similar in spirit to the variational wavefunction proposed by Fogler and Koulakov for round bubbles[17]. The direction of \mathbf{a} characterizes spatial orientation of the elongated electron bubble. The electron density of such an elongated bubble, projected on the $n = 2$ LL, is

$$\begin{aligned} \rho_{\xi, \mathbf{a}}(\mathbf{q}) = & e^{-\frac{q^2}{4}} \left[\left(1 - 2e^{-2a^2} a^2 \right) (1 + |\xi|^2) + 2(1 - 2a^2) e^{-2a^2} \Re e(\xi) \right]^{-1} \\ & \times \left\{ e^{i\mathbf{q} \cdot \mathbf{a}} \left(1 + |\xi|^2 - \frac{|\xi|^2 q^2}{2} \right) + e^{-i\mathbf{q} \cdot \mathbf{a}} \left(1 + |\xi|^2 - \frac{q^2}{2} \right) \right. \\ & - e^{-2a^2 + (\mathbf{q} \times \mathbf{a}) \cdot \hat{z}} \left[(2a^2 - (\mathbf{q} \times \mathbf{a}) \cdot \hat{z}) (1 + |\xi|^2) - 2(1 - 2a^2) \Re e \xi \right. \\ & \left. \left. + \frac{\xi q^2}{2} - 2\xi(\mathbf{q} \times \mathbf{a}) \cdot \hat{z} + i(1 - |\xi|^2) \mathbf{q} \cdot \mathbf{a} \right] \right. \\ & \left. - e^{-2a^2 + (\mathbf{a} \times \mathbf{q}) \cdot \hat{z}} \left[(2a^2 - (\mathbf{a} \times \mathbf{q}) \cdot \hat{z}) (1 + |\xi|^2) - 2(1 - 2a^2) \Re e \xi \right. \right. \\ & \left. \left. + \frac{\xi^* q^2}{2} - 2\xi^*(\mathbf{a} \times \mathbf{q}) \cdot \hat{z} + i(1 - |\xi|^2) \mathbf{q} \cdot \mathbf{a} \right] \right\}, \quad (\text{S23}) \end{aligned}$$

where $\bar{a} = a_x + ia_y$, and $a^* = a_x - ia_y$. In order to write down an asymptotic expression for the effective interaction between bubbles at different nodes of the two-electron bubble lattice taking into account elongation of bubbles, it is convenient to express the interaction in terms of elongations \mathbf{a}_i and effective dipole moments $\boldsymbol{\mu}_i$, which represent rotated and re-scaled \mathbf{a}_i . Retaining terms up to R_{ij}^{-3} for energy change due to elongations we obtain

$$\begin{aligned} \delta U_2(\mathbf{R}_{ij}) = & \frac{(\boldsymbol{\mu}_i - \boldsymbol{\mu}_j) \cdot \hat{\mathbf{R}}_{ij}}{R_{ij}^2} + \frac{\boldsymbol{\mu}_i \cdot \boldsymbol{\mu}_j - 3(\boldsymbol{\mu}_i \cdot \hat{\mathbf{R}}_{ij})(\boldsymbol{\mu}_j \cdot \hat{\mathbf{R}}_{ij})}{R_{ij}^3} \\ & + \frac{u(a_i, \xi_i) + u(a_j, \xi_j)}{R_{ij}^3} + \frac{v(a_i, \xi_i) \cos(2\phi_i - 2\theta_{ij}) + v(a_j, \xi_j) \cos(2\phi_j - 2\theta_{ij})}{R_{ij}^3} \end{aligned} \quad (\text{S24})$$

Here θ_{ij} is the phase of \mathbf{R}_{ij} , ϕ_i and ϕ_j are the phases of elongation vectors \mathbf{a}_i and \mathbf{a}_j for bubbles located at sites i and j respectively, $\hat{\mathbf{R}}_{ij} = \mathbf{R}_{ij}/R_{ij}$, and

$$\boldsymbol{\mu} = \frac{2\mathcal{R}(\mathbf{a})}{e^{2a^2} - 2a^2} \frac{\sqrt{1 - \left(\frac{2\Re e \xi}{1 + |\xi|^2} \right)^2}}{1 + \eta_1(a) \frac{2\Re e \xi}{1 + |\xi|^2}}, \quad (\text{S25})$$

$$u(a, \xi) = a^2 \frac{e^{2a^2} + 2a^2 (1 + |\xi|^2) - 2\eta_2(a) \Re e(\xi)}{e^{2a^2} - 2a^2 (1 + |\xi|^2) + 2\eta_1(a) \Re e(\xi)}, \quad (\text{S26})$$

$$v(a, \xi) = 3a^2 \frac{e^{2a^2} - 2a^2 + 2(1 + |\xi|^2) + 2\eta_3(a) \Re e(\xi)}{e^{2a^2} - 2a^2 (1 + |\xi|^2) + 2\eta_1(a) \Re e(\xi)}, \quad (\text{S27})$$

where the following notations have been used

$$\eta_1(a) = \frac{1 - 2a^2}{e^{2a^2} - 2a^2}, \quad (\text{S28})$$

$$\eta_2(a) = \frac{1 - 2a^2}{e^{2a^2} + 2a^2}, \quad (\text{S29})$$

$$\eta_3(a) = \frac{3 - 2a^2}{e^{2a^2} - 2a^2 + 2}, \quad (\text{S30})$$

and $\mathcal{R}(\mathbf{a})$ represents vector \mathbf{a} rotated by an angle $\phi_k = \arg(1 - |\xi|^2 + 2\Im m\xi)$. The above analytical expressions originate in the Hartree term of the potential (Eq. S3) because the contribution to the exchange potential (Eq. S3) behaves as $\exp(-R^2/4)$ and is neglected.

We consider two types of charge defects, one and three-electron bubble defects, in the presence of elongations. The wavefunction of a one-electron bubble is $u_{-2}(\mathbf{r})$, and has round shape. The asymptotic expansion of the contribution to interactions between a defect at site k and a two-electron bubble at site i due to elongations, with terms up to R_{ik}^{-3} is obtained from Eq. S4:

$$\delta U_1(\mathbf{R}_{ik}) = \frac{\boldsymbol{\mu}_i \hat{\mathbf{R}}_{ik}}{R_{ik}^2} + \frac{u(a_i, \xi_i) + v(a_i, \xi_i) \cos(2\phi_i - 2\theta_{ik})}{2R_{ik}^3}. \quad (\text{S31})$$

A three-electron defect, similarly to two-electron bubbles, has internal structure and nonuniform density. A wavefunction of a three-electron bubble is a Slater determinant made of u_{-2} , u_{-1} , and $u_{m=0}$. Exact structure and shape of these defects can be determined by minimizing the cohesive energy, however, as our numerical study shows, energetics and electron transport are primarily determined by elongations of the crystalline two-electron bubbles. Thus, the detailed structure of the $3\bar{e}$ bubble is not essential and we model it as having all three guiding centers on top of each other, just like three-electron bubbles have always been treated. A contribution to effective interaction of such a defect located at site k with a two-electron bubble at site i due to elongations is given by:

$$\delta U_3(\mathbf{R}_{ik}) = \frac{3\boldsymbol{\mu}_i \hat{\mathbf{R}}_{ik}}{R_{ik}^2} + \frac{3[u(a_i, \xi_i) + v(a_i, \xi_i) \cos(2\phi_i - 2\theta_{ik})]}{2R_{ik}^3}. \quad (\text{S32})$$

It is worth noting that due to the symmetry of triangular lattice $\sum_j \cos(\phi_i - \theta_{ij})/R_{ij}^n = 0$, where the summation runs over all sites of an ideal crystal and n is a positive integer. Also, the following result is used in what follows: $\alpha = \zeta_1 = w^3 \sum_j 1/R_{ij}^3 \approx 11.03$, where w is the lattice constant of the bubble crystal.

If a charge defect is embedded in the otherwise pristine system, the effective Hamiltonian in the presence of elongations of bubbles is derived using Eqs. S4 and S24-S32 and is given by Eq. 3 of the main paper

$$H^\pm = \sum_{i \neq k} \left[\mp \left[\frac{\boldsymbol{\mu}_i \hat{\mathbf{R}}_{ik}}{R_{ik}^2} + \frac{v_i}{2R_{ik}^3} \cos(2\varphi_i) \right] + U_f^\pm(i) \right] + \frac{1}{2} \sum_{i \neq j; i, j \neq k} \frac{\boldsymbol{\mu}_i \cdot \boldsymbol{\mu}_j - 3(\boldsymbol{\mu}_i \cdot \hat{\mathbf{R}}_{ij})(\boldsymbol{\mu}_j \cdot \hat{\mathbf{R}}_{ij})}{R_{ij}^3}, \quad (\text{S33})$$

where (+) corresponds to the presence of three- and (−) one-electron bubbles, $\varphi_i = \phi_i - \theta_{i,k}$, and the following notation is introduced

$$v_i = v(a_i, \xi_i), \quad (\text{S34})$$

$$U_f^\pm(i) = U_f^\pm(a_i, \xi_i), \quad (\text{S35})$$

where

$$U_f^\pm(a_i, \xi_i) = \left(\frac{\alpha}{w^3} \mp \frac{1}{2R_{ik}^3} \right) u(a_i, \xi) + \frac{1}{2} U(0, a_i, \xi_i), \quad (\text{S36})$$

and $U(0, a_i, \xi_i)$ is defined in Eq. S4. The first two terms of Eq. S33 represent an effective one-body (one-bubble) energy, the third one describes the formation energy at the bubble site i due to the presence of a defect, and the fourth term represents an effective interaction of orientations of bubbles.

In the presence of multiple defects located at sites k ,

$$\begin{aligned} H^\pm = & \sum_{i \neq k} \left[\sum_k \mp \left[\frac{\boldsymbol{\mu}_i \cdot \hat{\mathbf{R}}_{ik}}{R_{ik}^2} + \frac{v(a_i, \xi_i)}{2R_{ik}^3} \cos(2\varphi_i) \right] + U_f^\pm(a_i, \xi_i) \right] \\ & + \frac{1}{2} \sum_{i \neq j; i, j \neq k} \frac{\boldsymbol{\mu}_i \cdot \boldsymbol{\mu}_j - 3(\boldsymbol{\mu}_i \cdot \hat{\mathbf{R}}_{ij})(\boldsymbol{\mu}_j \cdot \hat{\mathbf{R}}_{ij})}{R_{ij}^3}. \end{aligned} \quad (\text{S37})$$

The ground state of a bubble system in the presence of charged defects can be obtained by minimizing the energy (Eq. S33). Assuming that $a/R \ll 1$, minimization of the first term provides a zeroth order result. The ground state of a bubble lattice with one-electron defect is obtained when $\phi_i - \theta_{ij} = 0, \pi$, and for a three-electron defect at $\phi_i - \theta_{ij} = \pi/2, 3\pi/2$. These states resemble “vortex” (antivortex) and “2D-hedgehog” (antihedgehog) textures. Vortex and antivortex texture of a one-electron defect are almost degenerate at relevant temperatures; similarly degenerate are hedgehog and antihedgehog energies. It is important to realize that the two-body interaction of Eq. S33 essentially represent an XY-model [24]. This is transparent if we take a continuum limit $\varphi_i \rightarrow \varphi_j$, where only $\cos(\varphi_i - \varphi_j)$ term is important. For the XY-model the vortex and hedgehog textures, which minimize the $1/R^2$ interaction of the bubble system with defects, constitute topological excitations. We note that XY-model physics characterizes dipole-dipole interactions of Eq. S33 even if continuum limit is not applied [33].

Minimization of energy (Eq. S33) in the limit of sufficiently large R_{ik} provides the values of the separation vector a_i and the mixing ξ_i . The effect of the interaction term is evaluated approximating a bubble located far away from the defect as being surrounded by bubbles with the same parameters a and ξ . The result of such minimization procedure is

$$a_i = \frac{w^2}{2^{\frac{1}{6}} 3^{\frac{1}{2}} \alpha^{\frac{3}{2}}} \left(\frac{1}{R_{ik}} \right)^{\frac{4}{3}} - \frac{27^{7/6} w^4}{3^{5/2} \alpha^{\frac{4}{3}}} \left(\frac{1}{R_{ik}} \right)^{\frac{8}{3}} \quad (\text{S38})$$

$$\xi_i^{3e} = -1 + i \frac{2w^2}{2\alpha^{\frac{2}{3}}} \left(\frac{1}{r} \right)^{4/3} \quad (\text{S39})$$

$$\xi_i^{1e} = -1 + \frac{2w^2}{2\alpha^{\frac{2}{3}}} \left(\frac{1}{r} \right)^{4/3}, \quad (\text{S40})$$

where superscripts 1e and 3e refer to one- and three-electron bubbles. In Fig.4b of the main paper, solid lines represent activation energies of one- and three-electron defects when decrease in energy due to elongations of crystalline bubbles is taken into account.

An important result of minimization of the energy is that textures associated with isolated defects of the bubble crystal are extended over a finite distance $L \sim 10w$ from the charge defect, where $w \sim 8\lambda$ is the lattice constant of the bubble crystal. As distance R_{ik} from the center of the charge defect increases, bubble elongation a_i decreases and parameter ξ_i in the wavefunction (2) is changing towards -1. At $R_{ik} \sim L$ symmetric wavefunction ($\xi_i \sim 1$) becomes energetically favorable, and elongations $a_i = 0$ (round bubbles) for $R_{ik} > L$.

At low temperatures the density of defects is low, defect separation is $> L$, textures from different defects do not overlap, and charged defects interact via Coulomb interaction. Consider first minimization of the interaction energy for defects of the same sign. Such defects form a superlattice superimposed on the bubble crystal, somewhat similar to the Wigner[3] or Abrikosov[12] lattice. Defects with opposite charges cannot easily approach and annihilate each other due to the difference in the symmetry of their textures, and we expect defect crystal to form even when charge defects of both signs are present. When temperature increases or filling factor is shifted from the center of the RIQHE state, the density of defects increases, see Fig. 4c of the main text. When defect separation becomes $< 2L$ textures of neighboring defects start to overlap and energy (S33) includes interaction between elongated bubbles belonging to different defects. This interaction is described by the XY model. In order to calculate energy caused by such interaction, we take the lower bound on the "exchange constant" J , which is the $\boldsymbol{\mu}_i \cdot \boldsymbol{\mu}_j$ term in (S33). We assume that J is defined by a characteristic magnitude of elongations $a \sim \lambda$ in the region where topological excitations overlap, which sets the lower bound to $J \sim e^2 a^2 / \kappa L^3$. The entropy of topological excitations is given then by[24]

$$E = (\pi J - 2T) \ln(\mathcal{L}/w), \quad (\text{S41})$$

where \mathcal{L} is the size of the system and the core of topological excitations is taken to be of the order of the bubble crystal lattice constant w . Such system must exhibit the Berezinski-Kosterlitz-Thouless (BKT) transition [10, 11] at $T_{KT} = \pi J/2$. However, the thermodynamic transition in the RIQHE regime differs from a conventional BKT transitions, e.g., discussed in [25], due to the finite size of topological defects L . At low densities there is no overlap between neighboring defects (their textures), and thus, the system cannot undergo the BKT transition. Temperature T_L , at which textures from neighboring defects begin to overlap, corresponds to defect density $1/(\pi L^2)$ is much higher than estimated $T_{KT} \approx 5$ mK. Thus, T_{KT} itself is not observed experimentally. The unbinding of topological defects at T_L required to avoid the divergence of logarithmic interactions (S41) constitutes *melting of the defect rather than the bubble crystal*. The T_L 's at different filling factors obtained in our calculations are very close to experimentally observed temperatures of metal-insulator transitions.

By using our analytical model, we have arrived at an estimate very close to the experimental data. On one hand, this should be taken with a grain of salt. We made a few assumptions in order to simplify our minimization procedures. In particular, we calculated first displacements of bubbles from lattice sites arising if bubbles are kept round, leading to results shown by dashed lines in Fig 4b of the main text. We then calculated the effect of elongations shown by solid lines in that figure assuming for simplicity that bubbles are arranged in a crystal lattice. Furthermore, Hamiltonian (S33) describing lattice bubbles around charged defects strictly speaking requires an account of additional terms with higher inverse power for bubbles very close to defects. We also discarded the effects of disorder in host heterostructure, which are known to result in lower experimentally observed activation energies as compared to theoretical predictions in quantum Hall studies. On the other

hand, the analytical model we use here would provide rigorous results for bigger separations between lattice bubbles. Furthermore, using our analytical model we can provide adequate analysis of the thermodynamics and transport, and in particular, correctly identify the symmetries of textures of lattice bubbles. It would be of interest to see how these textures appear in full numerical simulation taking into account effects of disorder in heterostructure.

After melting of the defect crystal, topological defects determine the resistivity as long as the bubble crystal is viable. The bubble crystal itself is going to melt, e.g., due to dislocations. We estimate the melting temperature of the bubble crystal using the Thouless formula [26, 27]:

$$\Gamma = \frac{4e^2\sqrt{\pi n_s}}{T\epsilon_r} = \frac{4\sqrt{2}e^2\sqrt{\pi}}{\sqrt[4]{3}Tw\epsilon_r}, \quad (\text{S42})$$

where n_s is the bubble density, w is the Wigner lattice constant, e is the electron charge, ϵ_r is the dielectric constant, T is the melting temperature. The factor 4 comes from the fact that in our case the bubbles have 2e charges. The dimensionless parameter $\Gamma = 78 - 130$ according to [26, 34–36]. Thus, we estimate the melting temperature of the bubble crystal $T \sim 400$ mK.

The effect of strain.

In order to evaluate the effect of strain on the elongation of bubbles we consider bubbles located relatively far from the defect charge, so we can neglect the term inversely proportional to R_{ij}^3 in the formation energy, Eq. S36. We limit interactions to the nearest neighbors and assume that elongations a_i vary slowly with the distance from charged defects. Due to large distance between the bubble and the defect, ϕ_i can be considered constant for the bubble and its nearest neighbors. Small deviations $\delta\phi_i$ of ϕ_i change the total energy, which, expanding Eq. S33, we express as $\delta E = \beta_i(\delta\phi_i)^2$, where

$$\beta_i = \frac{2}{R_{ik}^2} \frac{a}{e^{2a^2} - 2a^2} \frac{\sqrt{1 - \left(\frac{2\Re e\xi}{1+|\xi|^2}\right)^2}}{1 + \eta_1(a) \frac{2\Re e\xi}{1+|\xi|^2}}. \quad (\text{S43})$$

Addition of a shear strain $\epsilon_{xx} = -\epsilon_{yy} = \epsilon$ into the model is done similarly to the case of stripe phase [15] using the “deformed coordinate system” obtained by the transformation of coordinate system $x \rightarrow x(1 + \epsilon)$, $y \rightarrow y(1 - \epsilon)$. In this coordinate system the lattice is identical to the unstrained one, but the interaction potential becomes anisotropic:

$$V_{\text{HF}}(\mathbf{q}) \rightarrow V_{\text{HF}}\left(\sqrt{q_x^2(1 - \epsilon)^2 + q_y^2(1 + \epsilon)^2}\right) = V_{\text{HF}}(q) + \epsilon \frac{\partial V_{\text{HF}}}{\partial q} q \cos(2\phi_q) \quad (\text{S44})$$

The linear in strain contribution in the real space Hamiltonian can be written as $H_\epsilon = -\epsilon U_f^\epsilon(a, \xi) \cos(2\phi_i)$ with

$$U_f^\epsilon(a, \xi) = \int \frac{d^2\mathbf{q}}{(2\pi)^2} \rho_{\xi, a\hat{e}_x}^*(\mathbf{q}) \frac{\partial V_{\text{HF}}}{\partial q} q \cos(2\phi_q) \rho_{\xi, a\hat{e}_x}(\mathbf{q}). \quad (\text{S45})$$

Terms of the form $\sum_j f((R_{ij})^n)$ are unaffected by the presence of strain due to triangular lattice symmetry. Strain induces small rotations of the elongation of bubbles $\delta_{\phi_i}^\epsilon = \epsilon\gamma_i \sin(2\phi_i)$, where $\gamma_i = \frac{1}{\beta_i} U_f^\epsilon$.

The angles describing elongation vectors become

$$\phi_i^\pm = \frac{3\pi}{4} + \theta_{ik} \pm \left(\frac{\pi}{4} + \epsilon\gamma_i \sin(2\theta_{ik})\right), \quad (\text{S46})$$

where (+) corresponds to the hedgehog and (−) the vortex texture.

When the defect crystal melts due to overlap of textures, charges are free to hop from one site to another. However, at the same time the textured pattern has to readjust for the new center of the defect and elongated bubbles must rotate. The superposition matrix element between the initial state of a bubble characterized by an elongation vector \mathbf{a} and the rotated one with an elongation vector $\mathbf{a} + \delta\mathbf{a}$ is given by

$$p(\delta\mathbf{a}) = \langle \Psi_{\mathbf{a}}^*(\mathbf{r}_1, \mathbf{r}_2) | \Psi_{\mathbf{a}+\delta\mathbf{a}}(\mathbf{r}_1, \mathbf{r}_2) \rangle = \left\{ e^{i\mathbf{a} \times \delta\mathbf{a} - \frac{\delta\mathbf{a}^2}{2}} \left[\left(1 - \frac{\delta\mathbf{a}^2}{2} \right) (1 + |\xi|^2) - \Re e \xi \frac{\delta\mathbf{a}^2}{2} \right] - 2e^{i\delta\mathbf{a} \times \mathbf{a} - 2\mathbf{b}^2} [\mathbf{b}^2 (1 + |\xi|^2) - \Re e \xi (1 - 2\mathbf{b}^2)] \right\} \times \left[(1 - 2e^{-2a^2} a^2) (1 + |\xi|^2) + 2(1 - 2a^2) e^{-2a^2} \Re e(\xi) \right]^{-1}, \quad (\text{S47})$$

$\mathbf{b} = \mathbf{a} + \delta\mathbf{a}/2$. For small rotations $\delta\phi$ the rotation probability $|p|^2$ becomes $p(\delta\phi)^2 = 1 - p_0(a)(\delta\phi)^2$ where

$$p_0(a) = \left\{ 2a^6 (|\xi|^2 + 2\Re e \xi + 1) \left[(4e^{2a^2} + 1) (|\xi|^2 + 1) + 4\Re e \xi \right] + 2a^2 \Re e \xi (|\xi|^2 + 4\Re e \xi + 1) + a^4 e^{2a^2} \left[3(|\xi|^2 + 1)^2 - 2\Re e \xi (|\xi|^2 + 1) + 4(\Re e \xi)^2 \right] + e^{2a^2} a^2 \left[(|\xi|^2 + 1)^2 - 2(\Re e \xi)^2 \right] - 2a^4 (|\xi|^2 + 3\Re e \xi + 1) (|\xi|^2 + 4\Re e \xi + 1) - e^{4a^2} a^2 (|\xi|^2 + 1) (2|\xi|^2 + \Re e \xi + 2) \right\} \times \left[(e^{2a^2} - 2a^2) (1 + |\xi|^2) + 2(1 - 2a^2) \Re e(\xi) \right]^{-2}. \quad (\text{S48})$$

If a defect is displaced by a small distance δ along the \hat{x} direction, the angle $\theta_{i,k}$ changes by $\sin \theta_{i,k}/R_{i,k}\delta$, while if the defect moves along \hat{y} direction the change is $-\cos \theta_{i,k}/R_{i,k}\delta$. Combining these expressions with the phase of elongation vector given by Eq. S46 we find the change in angles ϕ_i for a hopping event

$$\delta_x \phi_i^\pm = +[1 \pm \epsilon \gamma_i \cos(2\theta_{i,k})] \frac{w \sin \theta_{i,k}}{R_{i,k}}, \quad (\text{S49})$$

$$\delta_y \phi_i^\pm = -[1 \pm \epsilon \gamma_i \cos(2\theta_{i,k})] \frac{w \cos \theta_{i,k}}{R_{i,k}}. \quad (\text{S50})$$

Introducing these quantities into matrix elements of Eq. S48, we find

$$|p_s^\pm(\delta\phi_i)|^2 = 1 - \frac{w^2}{R_{i,k}^2} p_0 [1 \pm 2\epsilon \gamma_i \cos(2\theta_{i,k})] \sin^2 \left(\theta_{i,k} + (1+s) \frac{\pi}{4} \right), \quad (\text{S51})$$

where $s = -1$ corresponds to the hopping of the defect along \hat{x} and $s = 1$ along \hat{y} direction.

The conductivity $\sigma_{xx(yy)}$ is proportional to the square of the matrix element of position (displacement) operator $r_{x(y)}$, which is proportional to the product of all $|p(\delta\phi_i)|^2$. Ratio between peaks due to $1\bar{e}$ and $3\bar{e}$ defects is given by

$$\frac{\sigma_{1e}}{\sigma_{3e}} = \prod_i \frac{1 - \frac{w^2}{R_{i,k}^2} p_0 [1 - 2\epsilon \gamma_i \cos(2\theta_{i,k})] \sin^2 \left(\theta_{i,k} + (1+s) \frac{\pi}{4} \right)}{1 - \frac{w^2}{R_{i,k}^2} p_0 [1 + 2\epsilon \gamma_i \cos(2\theta_{i,k})] \sin^2 \left(\theta_{i,k} + (1+s) \frac{\pi}{4} \right)}. \quad (\text{S52})$$

We see that although strain leads to a small change of overlap between two bubbles, the effect on the motion of the whole topological defect, dependent on overlap of many bubbles,

is a giant effect. Thus, our model explains both symmetry aspects and unusually large magnitude of the strain effect on resistivity observed experimentally.

-
- [29] H. Fukuyama, P. M. Platzman, and P. W. Anderson, “Two-dimensional electron gas in a strong magnetic field,” *Phys. Rev. B* **19**, 5211–5217 (1979).
 - [30] Naokazu Shibata and Daijiro Yoshioka, “Ground-state phase diagram of 2D electrons in a high Landau level: A density-matrix renormalization group study,” *Phys. Rev. Lett.* **86**, 5755–5758 (2001).
 - [31] Daijiro Yoshioka and Naokazu Shibata, “DMRG study of the ground state at higher Landau levels: stripes, bubbles and the Wigner crystal,” *Physica E* **12**, 43 – 45 (2002).
 - [32] A. M. Ettouhami, F. D. Klironomos, and A. T. Dorsey, “Possible new bubble phases of two-dimensional electrons in higher Landau levels,” *Int. J. Mod. Phys. B* **18**, 3645–3648 (2004).
 - [33] Sona Prakash and Christopher L. Henley, “Ordering due to disorder in dipolar magnets on two-dimensional lattices,” *Phys. Rev. B* **42**, 6574 (1990).
 - [34] R W Hockney and T R Brown, “A lambda transition in a classical electron film,” *Journal of Physics C: Solid State Physics* **8**, 1813.
 - [35] R. C. Gann, Sudip Chakravarty, and G. V. Chester, “Monte carlo simulation of the classical two-dimensional one-component plasma,” *Phys. Rev. B* **20**, 326–344 (1979).
 - [36] R. H. Morf, “Temperature dependence of the shear modulus and melting of the two-dimensional electron solid,” *Phys. Rev. Lett.* **43**, 931–935 (1979).

Extended Methods

NEW TOPOLOGICAL EXCITATIONS AND MELTING TRANSITIONS IN QUANTUM HALL SYSTEMS

Tzu-ging Lin, George Simion, John D. Watson, Michael J. Manfra, Gabor A. Csathy, Yuli Lyanda-Geller, and Leonid P. Rokhinson

I. THERMALLY-INDUCED STRAIN.

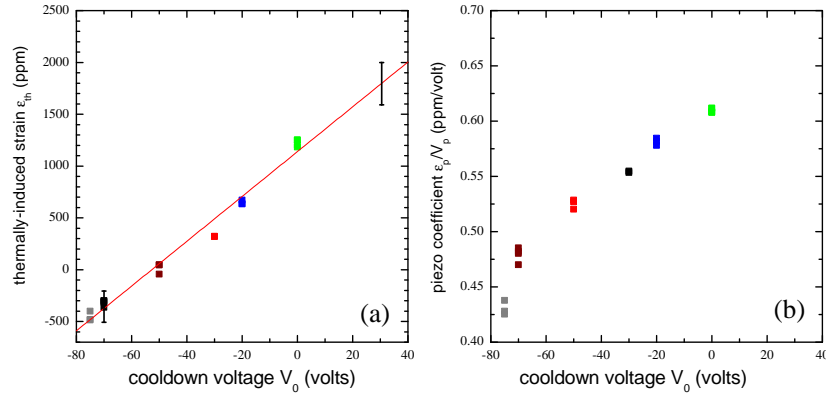


FIG. E1. **Thermally induced strain.** Thermally induced strain can be controlled by applying voltage V_0 on the transducer during cooldown. The piezo coefficient has weak dependence on V_0 .

A PZT-based multilayer piezoelectric transducer has very anisotropic thermal expansion coefficients (+3/−1 ppm/deg near room temperature) along and perpendicular to the polling direction. The residual thermally induced strain ϵ_{th} (at $V_p = 0$) can be controlled by voltage V_0 applied to the transducer during cooldown. A dependence of $\epsilon_{th}(V_0)$ is plotted in Fig. E1, measured with a bi-axial strain gauge. There is almost no thermal expansion/contraction and no hysteresis in the $\epsilon_p(V_p)$ characteristic below 10 K.